# Multi-Layer Planar Near Field Holography using MEMS microphone arrays in a noisy environment

M.J.L.H. Thomassen, P.C.W.. Sommen, H. Nijmeijer
Eindhoven University of Technology, P.O. Box 513, 5600 MB Eindhoven, The Netherlands

R. Scholte
Sorama B.V. Torenallee 20, Eindhoven, The Netherlands

**Summary**
Near-field acoustic measurements in noisy environments suffer from interference generated by undesired sources, especially when they are located close to the measurement equipment. Planar Near-field Acoustic Holography (PNAH) using a single layer pressure sensor array, is a proven method for determining sound pressure fields in high detail at the source of vibrating objects, however, its accuracy is impacted when an undesired source is present closely behind the measurement array. This paper presents a method for performing PNAH using an arbitrary number of MEMS pressure sensor arrays using a Multi-Layer method not bound to one or two measurement planes. The results are demonstrated by measurements using two MEMS microphone arrays which show that Multi-Layer PNAH is a qualitative improvement over single layer PNAH in both noisy but also non-noisy environments and that it can be easily implemented and used in practice by utilizing MEMS technology.

**PACS no. 43.58.-e, 43.60.Fg, 43.60.Sx**

## 1. Introduction

Planar Near-field Acoustic Holography (PNAH) [1] has been proven to be accurate, fast and practically feasible for the analysis of sound pressure, particle velocity and sound intensity [2]. PNAH assumes a source-free space behind a single measurement plane as illustrated in Figure 1a. This assumption is not valid in many practical situations, in which disturbing sources behind the measurement plane require a multi-layer setup to obtain accurate results. Two situations arise in which the PNAH assumption of a source free half space does not hold:

1. Sound sources are located across one another, for example two active generatortrs placed next to each other or a person speaking behind the measurement plane during a measurement.
2. Sound waves emitted by an object of interest will reflect off of most surfaces in the surroundings of the source, for example an active ventilation system mounted close to a concrete wall.

A combination of the two is also possible. The second situation has been researched by Collins [3] and Moers [4], Collins [3] briefly touches on the first situation but does not explore it further. Several methods have been proposed for performing measurements in the presence of reflecting surroundings or disturbing sources, mainly based on the Statistically Optimal NAH technique as in [5, 6]. Fourier-based Dual Layer PNAH techniques have previously been discussed in [7, 3], based on the approach of Tamura [8]. The separation method as described by Havranek et al. [7] only treats sources originating in front of the measurement planes. Collins [3] formulates equations for both sources originating in front and behind the measurement planes, but does not combine the two. This paper aims to research the improvements possible by using mutiple pressure sensor layers in both envirionments with and without a disturbing source and compare the results of the seperation method with calculating the, actual, entire sound-field. We cover Dual-Layer PNAH for pressure measurements in Section 2 and extends the theory to more then two planes: Multi-Layer PNAH. Due to practical limitations, it is implemented using a Dual-Layer MEMS microphone array in Section 3. Section 4 shows measurement results. Conclusions are provided in Section 5 followed by a short discussion.

## 2. Dual- and Multi-Layer PNAH

Assume a situation described by two infinitely large half-spaces containing sources, $S_1$ and $S_2$ respectively, and a source-free space in between, as illustrated in Figure 1b. To obtain the sound pressure field at the

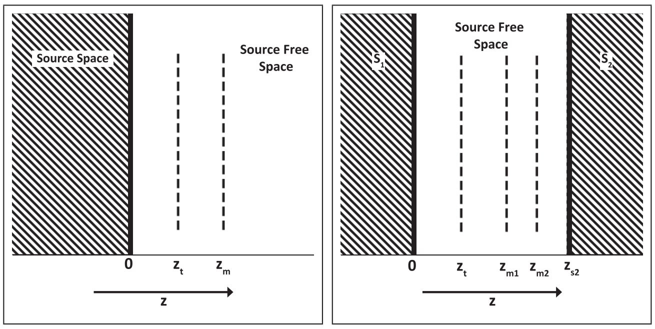


(a) Setup for PNAH. (b) Setup for Multi Layer PNAH with two layers.

Figure 1: Side views of measurement setups for both PNAH and MLPNAH

target plane $z_t$, a source separation method in k-space as done by Havranek et al. [7] and Collins [3] is performed. Using the same approach as Collins [3], the following notation of the source separation method is proposed:

$$\begin{aligned}\mathbf{P}(z_{m_1}) &= \mathbf{P_{S_1}}(z_t) \odot e^{-i\mathbf{k_z}(z_t - z_{m_1})} + \mathbf{P_{S_2}}(z_t) \odot e^{i\mathbf{k_z}(z_t - z_{m_1})} \\ \mathbf{P}(z_{m_2}) &= \mathbf{P_{S_1}}(z_t) \odot e^{-i\mathbf{k_z}(z_t - z_{m_2})} + \mathbf{P_{S_2}}(z_t) \odot e^{i\mathbf{k_z}(z_t - z_{m_2})},\end{aligned} \tag{1}$$

where $\mathbf{k_z}$ is the (vector) wave number in the z direction, $\mathbf{P}(z_{m_1})$ and $\mathbf{P}(z_{m_2})$ are the (vector) sound pressures on the measurement planes and $\mathbf{P_{S_1}}(z_t)$ and $\mathbf{P_{S_2}}(z_t)$ are the (vector) sound pressures on the target plane induced by sources in $S_1$ and $S_2$ respectively and $\odot$ denotes elementwise multiplication. In order to solve for $\mathbf{P_{S_1}}(z_t)$ and $\mathbf{P_{S_2}}(z_t)$ , Equation (1) can be written as:

$$\mathbf{P_m} = \mathbf{G}\mathbf{P_t}. \tag{2}$$

where

$$\begin{aligned}\mathbf{P_m} &= \begin{bmatrix} \mathbf{P}(z_{m_1}) \\ \mathbf{P}(z_{m_2}) \end{bmatrix} \\ \mathbf{P_t} &= \begin{bmatrix} \mathbf{P}_{S_1}(z_t) \\ \mathbf{P}_{S_2}(z_t) \end{bmatrix} \\ \mathbf{G} &= \begin{bmatrix} \mathrm{diag}(e^{-i\mathbf{k_z}(z_t - z_{m_1})}) & \mathrm{diag}(e^{i\mathbf{k_z}(z_t - z_{m_1})}) \\ \mathrm{diag}(e^{-i\mathbf{k_z}(z_t - z_{m_2})}) & \mathrm{diag}(e^{i\mathbf{k_z}(z_t - z_{m_2})}) \end{bmatrix}.\end{aligned}$$

The solution to the dual layer problem becomes:

$$\mathbf{P_t} = \mathbf{G}^{-1}\mathbf{P_m}. \tag{3}$$

From $\mathbf{P_t}$ the effects of $S_1$ or $S_2$ (source separation) on the target plane are obtained and the complete sound pressure field (full field) is given by:

$$\mathbf{P}(z_t) = \mathbf{P_{S_1}}(z_t) + \mathbf{P_{S_2}}(z_t). \tag{4}$$

The reader will notice that an arbitrary number of measurement planes can be defined in $\mathbf{P_m}$. However, even for the dual layer case, the propagation matrix $\mathbf{G}$ is not full column rank since there is at least one $k_{zi} = 0$ (on the radiation circle). Our solution to this problem is described in Section 3.2.1. Furthermore, $\mathbf{G}$ is guaranteed to be full row rank since two measurement planes can never occupy the same position. Now using our solution, with $\hat{\mathbf{G}}$ denoting the full rank, modified version of $\mathbf{G}$, the left pseudoinverse is used for determining the least-squares solution:

$$\mathbf{P_t} = (\hat{\mathbf{G}}^T\hat{\mathbf{G}})^{-1}\hat{\mathbf{G}}^T\mathbf{P}_m. \tag{5}$$

Equation (5) is the Multi-Layer PNAH (MLPNAH) equation.

## 3. Implementation of MLPNAH

Using a multi layer technique introduces some additional problem to the already existing ones encountered when using a single layer technique.

### 3.1. Conversion to K-Space

Conversion from measured pressure to the wavenumber domain is performed in the same manner as in [9] using Linear Predictive Border-Padding (LPBP), for each layer individually. According to Collins [3], the desired source's amplitude should exceed the undesired source's to prevent a reconstruction error. This error can be reduced using border padding to increase the k-space resolution by creating more (virtual) measurement points as illustrated in Figure 2. The border padded hologram in Figure 2c results in finer sampling in k-space compared to Figure 2b. Therefore, the propagation formula is evaluated for more and smaller bins, more accurately representing the actual k-space distrubution as shown in Figure 2a. This facilitates the separation of sources which would otherwise be located in the same bin. Figure 3 shows a reconstruction using MLPNAH with a single disturbing plane wave present behind the two measurement arrays, when using a border padding factor of two and eight respectively. The difference between the two and the actual source pressure is clearly visible. Care should be taken since this method, while improving results, does not guarantee a completely accurate reconstruction as very small differences in source distrubtion can still overlap due to k-space discretization.

### 3.2. Inverse propagation

#### 3.2.1. Radiation Circle Singularity

In Equation (5), $\mathbf{G}$ is not full rank because $k_{zi} = 0$ on the radiation circle. In [7] a solution is proposed based on the averaged Green's function approach by Williams [10]. In this paper, the continuum of $k_z$ is subdivided into spatial frequency bins that contains a

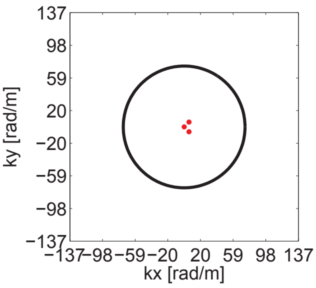


(a) Analytical k-space distribution showing 3 different peaks.

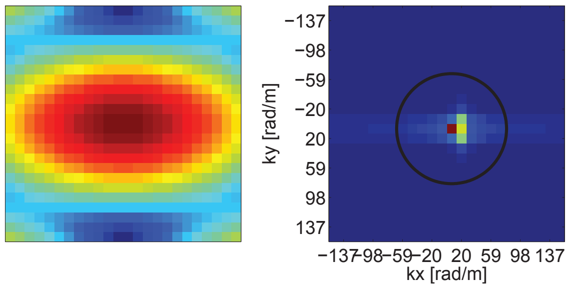


(b) Measured aperture (left) and corresponding k-space (right). Only a single peak is visible in k-space.

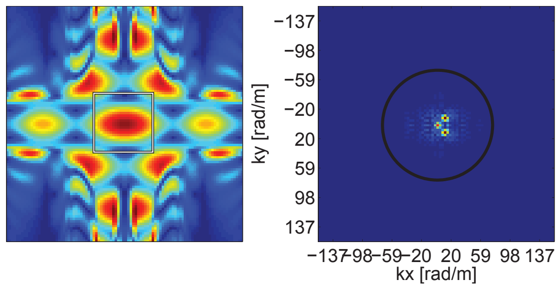


(c) Aperture (rectangle) expanded four times with LPBP (left) and corresponding k-space (right). All three peaks are visible in k-space.

Figure 2: Illustration of the effects of borderpadding in the spatial domain and k-space. Three plane waves are simulated. Each point in these images represents the corresponding sensor.

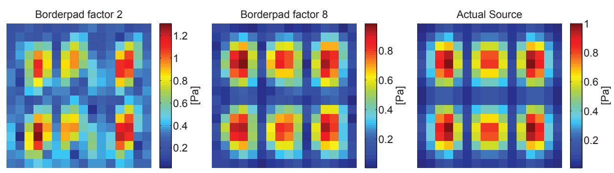


Figure 3: Reconstruction of vibrating plate with plane wave disturbance. Border padding factor of 2 (left) and 8 (middle) compared with actual source (right). Each point in these images represents the corresponding sensor.

span of values $\Delta k$ wide in both $k_x$ and $k_y$ direction, where $\Delta k = \frac{2\pi}{L}$ and $L$ is the size of the measurement aperture. When $k_{zi}$ is close to or exactly zero in one of the bins, that specific bin is unproportionally amplified as illustrated in Figure 4a. The value of $k_{zi}$ in a two-dimensional bin is therefore calculated as the mean value of the four corner points of that bin for calculation of all propagators. Now, $k_{zi}$ is an average of the values that a bin on the radiation circle contains, instead of $k_{zi} = 0$ when the center of the bin is exactly on the radiation circle. With this solution, $k_{zi} \neq 0$ and $\hat{\mathbf{G}}$ is now the full rank matrix in Equation (5). Results are shown in Figure 4b .

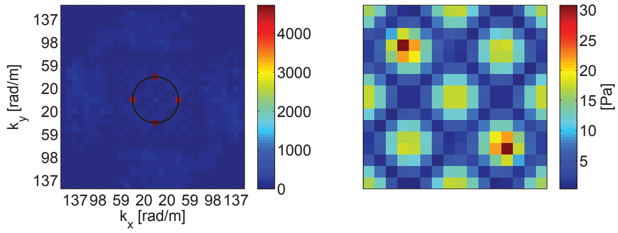


(a) Singularity in k-space pressure bins (left) on the radiation circle cause the reconstruction (right) to fail.

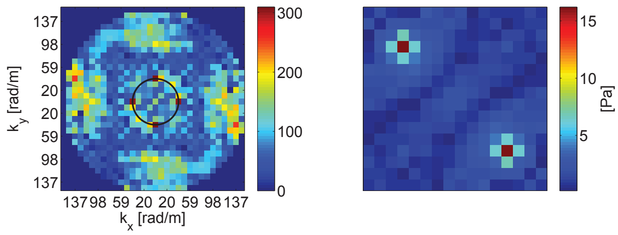


(b) Averaging of $k_z$ reduces singularities in k-space (left) resulting in a more accurate reconstruction (right).

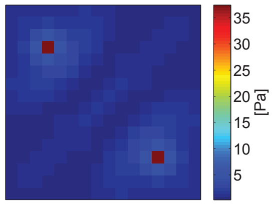


(c) Actual source pressure distribution.

Figure 4: Illustration of the propagator singularity on the radiation circle.

#### 3.2.2. Regularization

Regularization is also necessary in MLPNAH when any of the exponents in the propagation matrix cause an amplitude increase for evanescent waves during propagation. It can be shown that no regularisation is needed when propagating to a plane in between the measurement planes. For all other locations regularization is required. The Modified Exponential Filter from [11] is used tot his end. The regularization filter is applied to all layers in the implementation used in this paper. Tests have shown that keeping the cut-off

Table I: Algorithm parameters for Simulations

| | |
|---|---|
| Linear Predictive Filter Order [9] | 6 |
| Border Padding Factor | 8 |
| Spatial Zero Padding Factor | 4 |
| K-Space Zero Padding Factor | 4 |
| Spatial Window | Tukey $r = 0.875$ |

$k_{co}$ and slope $\phi$ filter parameters equal for both layers leads to the best results, because in most cases the same spatial information is present in both layers.

## 4. Measurement Results

Measurements have been performed to show MLPNAH results and feasibility in a practical setup. The two types of sources treated are point sources and a vibrating plate. For the acquisition of data, two Sorama 64-microphone MEMS arrays have been used, placed in parallel to each other, as illustrated in Figure 1b. Both arrays have 64 microphones in an eight by eight grid with 0.02 m spacing such that the total aperture is 0.14 x 0.14 m. The rear measurement plane is located at z = 0.10m, the front measurement plane is varied in steps of 0.005 m from z = 0.05m to z = 0.08m. The algorithm parameters are shown in table I. The reference planes for all measurements are created by performing a measurement at 0.025 m without any disturbing sources activated and calculated towards the source plane at 0.00 m using PNAH. To ensure correct measurement of the point sources, they have been placed in the front of a microphone in the array such that the point source's peaks are always present in a measurement.

### 4.1. Error Measurement

Different aspects of quality can be considered by choosing different error measures. Scholte [2], van Dalen [12] and Moers [4, 13] propose using a Root Mean Square (RMS) measure. A problem, noted by Moers, arises with this measure when sound pressure fields contain zero crossings. These cause high errors using an RMS or similar measure, while the actual visible result might still be acceptable. In order to assess the qualitative error of reconstruction, a novel error measure is presented, the Normalised Sum of Absolute Differences (NSAD), derived from the Sum of Absolute Differences (SAD) often used in image processing [14]. It does not suffer from singularities at zero crossings in the reconstruction or reference and provides a way to measure visual similarities for qualitative analysis. Errors presented in this paper will use both the RMS (as in [13] with a threshold of 1/1024th of the

Table III: Regularization filter parameters for Measurement 2

| Front plane position [m] | $k_{co}$[rad/m] | $\phi$[-] |
|---|---|---|
| 0.050 | 80 | 1 |
| 0.055 | 75 | 0.9 |
| 0.060 | 72 | 1 |
| 0.065 | 72 | 0.9 |
| 0.070 | 67 | 0.5 |
| 0.075 | 65 | 0.7 |
| 0.080 | 65 | 0.66 |

mean of the absolute reference) and NSAD. Both errors are combined to form the total error measure $E_{tot}$ for clarity and convenience. All formulas are shown in table II.

Table II: Error Measures

$$RMS(\tilde{p_h}, \tilde{p_r}) = \sqrt{\frac{1}{MN} \sum_{m=0}^{M-1} \sum_{n=0}^{N-1} \frac{|\tilde{p_r} - \tilde{p_h}|^2_{m,n}}{|\tilde{p_r}|^2_{m,n}}}$$

$$NSAD(\tilde{p_h}, \tilde{p_r}) = \frac{1}{MN} \sum_{m=0}^{M-1} \sum_{n=0}^{N-1} \left| \frac{|\tilde{p_r}|_{m,n} - |\tilde{p_h}|_{m,n}}{\max(|\tilde{p_r}|)} \right|$$

$$E_{tot}(\tilde{p_h}, \tilde{p_r}) = \sqrt{RMS(\tilde{p_h}, \tilde{p_r}) \times NSAD(\tilde{p_h}, \tilde{p_r})}$$

Here, $\tilde{p_r}$ is the reference and $\tilde{p_h}$ is the hologram to obtain the error for, both $M * N$ 2-dimensional arrays of complex pressure values.

All results shown below include those of PNAH, dual-layer MLPNAH source separation (indicated as DLPNAH Sep.) and dual-layer MLPNAH full field (indicated as DLPNAH Full).

### 4.2. Single source region

#### 4.2.1. Measurement 1: Point sources

Two point sources emitting a frequency of 1000 Hz are placed in front of the measurement array, both at $z = 0$m. Table III lists parametes and Figures 5 and 7 show the results. Figure 6 shows the reference plane.

### 4.3. Dual source regions

#### 4.3.1. Measurement 2: Point source with disturbing source

Two point sources emitting a frequency of 1000 Hz have been measured. One in front of the array at $z = 0$m, one behind the array at $z = 0.14$m. Table IV lists parrameters and in Figures 8 and 10 show the results. Figure 9 shows the reference plane.

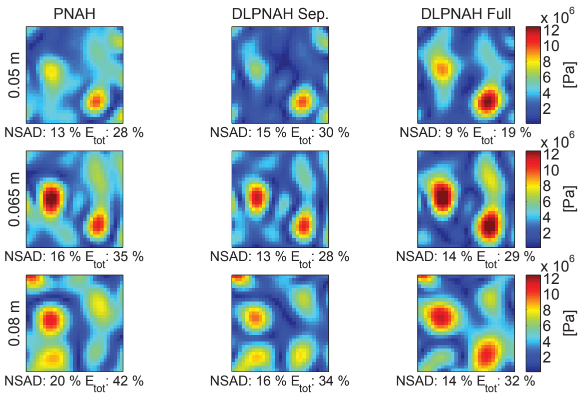


Figure 5: Measurement 1 results for front plane position 0.05, 0.065 and 0.08 m. Two point sources are located in front of the measurement planes.

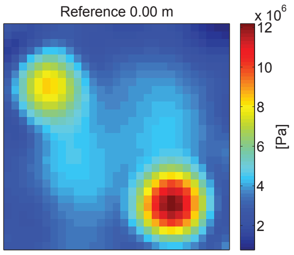


Figure 6: Reference plane pressure distribution for measurement 1.

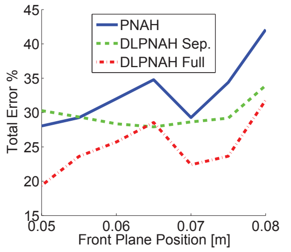


Figure 7: Total reconstruction error vs front plane position for measurement 1.

Table IV: Regularization filter parameters for Measurement 2

| Front plane position [m] | $k_{co}$[rad/m] | $\phi$[-] |
|---|---|---|
| 0.050 | 65 | 0.15 |
| 0.055 | 65 | 0.5 |
| 0.060 | 65 | 0.5 |
| 0.065 | 60 | 0.5 |
| 0.070 | 60 | 0.5 |
| 0.075 | 55 | 0.5 |
| 0.080 | 50 | 0.6 |

#### 4.3.2. Measurement 3: Vibrating plate with disturbing source

A vibrating plate has been measured at 259 Hz, located at $z = 0$m with one point source behind the measurement array located at $z = 0.14$m. Table V lists parameters and Figures 11 and 13 show the results. Figure 12 shows the reference plane.

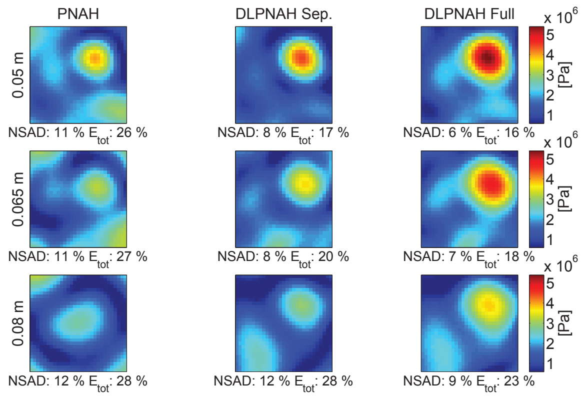


Figure 8: Measurement 2 results for front plane position 0.05, 0.065 and 0.08 m. One point source is located at the top right in front of the measurement planes and one at the bottom left behind the measurement planes.

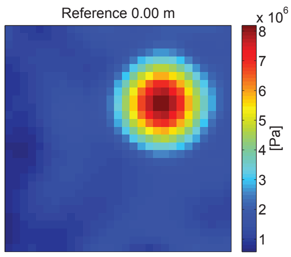


Figure 9: Reference plane pressure distribution for measurement 2.

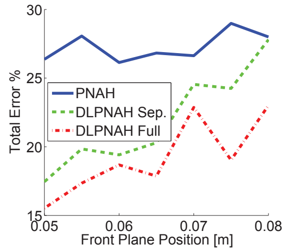


Figure 10: Total reconstruction error vs front plane position for measurement 2.

Table V: Regularization filter parameters for Measurement 3

| Front plane position [m] | $k_{co}$[rad/m] | $\phi$[-] |
|---|---|---|
| 0.050 - 0.065 | 40 | 0.1 |
| 0.070 | 35 | 0.1 |
| 0.075 | 30 | 0.1 |
| 0.080 | 30 | 0.1 |

## 5. Conclusions and Discussion

The Multi-Layer PNAH algorithm has been successfully impelemented using two layers. However, an arbitary number of layers can be used, leading to a least squares solution for inverse-propagation. The construction of a MEMS microphone array with more then two layers is ongoing and made possible by current advances in technology such as flex-rigid printed circuit boards and bottom-port MEMS.

Measurement results show that using the full field method in MLPNAH consistently leads to better re-

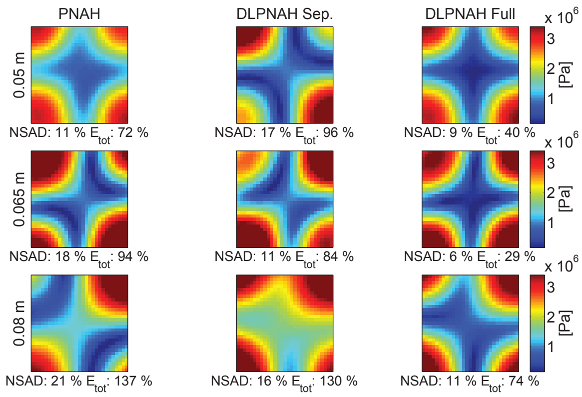


Figure 11: Measurement 3 results for front plane position 0.05, 0.065 and 0.08 m. A vibrating plate is located in front of the measurement planes and a point source is located behind the measurement planes.

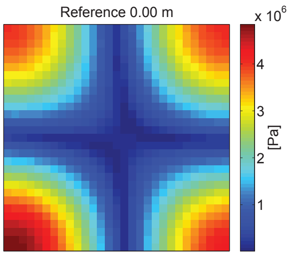


Figure 12: Reference plane pressure distribution for measurement 3.

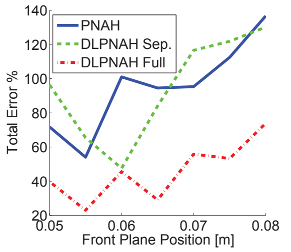


Figure 13: Total reconstruction error vs front plane position for measurement 3.

constructions than using regular PNAH or the source separation MLPNAH method. Figure 7 indicates that full-field MLPNAH results in the lowest error of all three methods, even with only sources present in front of the measurement array. In theory, under ideal circumstances, PNAH and MLPNAH should perform equally well here, however, in the MLPNAH measurements twice as much microphones have been used which leads to an effective increase in singal-to-noise ratio which comes 'for free' in a muli-layer approach. Measurement results in Figure 5 do show a clear difference between the three methods, especially as the distance between source and front measurement array gets larger. Furthermore, measurement results with sources present behind the measurement arrays in Figures 8 and 13 respectively, show that source separation performs worse than the full field method and even PNAH at some distances in the measurement of Section (4.3.2). This can be partially attibuted to the separation method removing some energy from the desired source distribution when separating it from the undesired source in k-space as described in section 3.1.

The feasibility of using Sorama's MEMS array technology to construct a dual layer microphone array to perform practical measurements in combination with MLPNAH has been shown. The most important contribution is the solution for an arbirary number of layers, enabling construction of a more accurate measurement device with multiple MEMS arrays. Further research into this topic needs to be performed to verify numerical stability for this method and practical tests should validate exact accuracy aswell as the influences of the physical structure of a multi-layer array on the sound-field.

## References

[1] E. G. Williams and J. D. Maynard. Holographic imaging without the wavelength resolution limit. *Phys. Rev. Lett.*, 45:554–557, 1980.

[2] R. Scholte. *Fourier Based High-resolution Near-Field Sound Imaging*. PhD thesis, University of Technology Eindhoven, 2008.

[3] Z. A. Collins. *Improved Measurement and Separation Technique for Interior Near-field Acoustical Holography*. PhD thesis, Brigham Young University, 2010.

[4] E. M. T. Moers, I. Lopez Arteaga, P.L. van Dalen, and R. Scholte. Detection of plate vibration modes by means of near-field acoustic holography in the presence of reflective surfaces. 2012.

[5] E. Fernandez-Grande and F. Jacobsen. Sound field separation with a double layer velocity transducer array. *J. Acoust. Soc. Am.*, 130:5–8, 2011.

[6] F. Jacobsen and V. Jaud X. Chen. A comparison of statistically optimized near field acoustic holography using single layer pressure-velocity measurements and using double layer pressure measurements. *J. Acoust. Soc. Am.*, 123:1842–1845, 2008.

[7] Z. Havranek and L. Bejcek. Verification of the double layer holographic array for extraction of sound fields in reverberant conditions. 2006.

[8] M. Tamura. Spatial fourier transform method of measuring reflection coefficients at oblique incidence. i: Theory and numerical examples. *J. Acoust. Soc. Am.*, 88:2259–2264, 1990.

[9] R. Scholte, I. Lopez, N.B. Roozen, and H. Nijmeijer. Truncated aperture extrapolation for fourier-based near-field acoustic holography by means of border-padding. *J. Acoust. Soc. Am.*, 125:3844–3854, 2009.

[10] E. G. Williams and J. D. Maynard. Numerical evaluation of the rayleigh integral for planar radiators using the fft. *J. Acoust. Soc. Am.*, 72:2020–2030, 1982.

[11] R. Scholte, I. Lopez, N. B. Roozen, and H. Nijmeijer. Wavenumber domain regularization for near-field acoustic holography by means of modified filter functions and cut-off and slope iteration. *Acta Acustica united with Acustica*, 94:339–348, 2008.

[12] P.L. van Dalen. Transient planar near-field acoustic holography. Master's thesis, Univesity of Technology Eindhoven, Dept. of Mechanical Engineering, 2012.

[13] E. M.T. Moers, I. Lopez-Arteaga, H. Nijmeijer, and R. Scholte. Accuracy assessment of planar near-field acoustical holography applied to non-resonant vibration imaging. 2013.

[14] G. de Haan. *Digital Video: Post Processing*. Royal Philips Electronics, 2006.